Life-Cycle Performance Assessment of Aging Bridges Subjected to Tsunami Hazards

Ji-Gang Xu[1]; De-Cheng Feng, A.M.ASCE[2]; and Gang Wu[3]

Abstract: Coastal reinforced concrete (RC) bridges have the potential to be subjected to tsunami hazards within their service life. On the other hand, the time-dependent chloride-induced corrosion will degrade the performance of the bridges. Few efforts have been made to investigate the life-cycle performance of deteriorating RC bridges subjected to tsunami hazards. In this paper, the time-dependent collapse fragility analysis is conducted to investigate the life-cycle performance of deteriorating RC bridges subjected to tsunami hazards. With corrosion modeling, the time-dependent deterioration of material properties as well as shear capacity deterioration of the columns are considered. Uncertainties from materials are accounted for in developing numerical bridge models. Nonlinear tsunami pushover analysis is used to investigate the bridge damage under tsunami loading. Tsunami collapse failure curves are constructed assuming a lognormal distribution, and the time-dependent tsunami collapse fragility curves can be efficiently calculated with the quadratic model for the median and standard deviation of tsunami intensity, that is, flow velocity. Time-dependent collapse fragility analysis is conducted for a three-span, two-column bent RC bridge. Results indicate that the bridge columns can fail in shear for low inundation depth flow and high corrosion levels. Collapse failure probability of the bridge increases with the flow depth and a clear jump of collapse failure probability for inundation depth from below to above the deck can be observed. The collapse failure probability also increases over time due to corrosion effects. **DOI: 10.1061/(ASCE)BE.1943-5592.0001711**.

Author keywords: RC bridge; Life-cycle performance; Tsunami hazard; Corrosion; Fragility analysis.

Introduction

Earthquake-triggered tsunami could be a great threat to coastal communities. Recent tsunami events, such as the 2004 Indian Ocean tsunami and the 2011 East Japan tsunami, caused severe consequences for communities along coastlines. For instance, based on the post-disaster investigation data, the 2004 Indian Ocean tsunami caused about 230,000 people deaths (Leelawat et al. 2016) and the 2011 East Japan tsunami event induced thousands of casualties as well as approximately $200 billion in economic losses (Kajitani et al. 2013). A great number of structures and infrastructures were damaged due to tsunami floods. More than 120,000 buildings were destroyed during the 2011 East Japan tsunami, and more than 300 bridges were heavily damaged (Akiyama et al. 2012). Although most of the coastal bridges could survive during the earthquake, they were totally damaged by the tsunami (Yim et al. 2015). Thus, it is of great importance to investigate the performance of bridges under tsunami hazards.

Tsunami flow could induce large forces on bridge systems and cause significant damage to coastal bridges. Research efforts on the assessment of tsunami loading effects on bridges systems has increased in recent years. Some studies tried to evaluate the tsunami loading on bridge columns. Arnason et al. (2009) and Shafiei et al. (2016) conducted experimental studies in order to evaluate the tsunami forces imposed on columns, and Wei et al. (2015) and Asadollahi et al. (2019) numerically investigated the tsunami forces imposed on columns. However, when the tsunami flow depth reached to the bridge deck, the tsunami flow could induce large forces on bridge superstructures. The experimental studies (Lau et al. 2011; Hayashi 2013) and numerical studies (Bricker and Nakayama 2014; Azadbakht and Yim 2015; Xu and Cai 2015) reveal that tsunami flow could induce large horizontal forces on the bridge decks or girders. Meanwhile, the tsunami flow could induce large vertical uplift forces that cause large overturning moment on the bridge superstructures, and hence the bridges could be easily damaged by the tsunami flow. In addition, some recent studies (Istrati et al. 2018; Winter et al. 2018; Istrati and Buckle 2019) highlight the importance of evaluating the distribution of tsunami forces on individual components in addition to the total tsunami loading due to the complex failure mechanism of bridge superstructures under tsunami flow. These studies could help to understand the damage effects of tsunami loading on coastal bridges.

In order to quantify the damage effects of tsunami loading on bridges, tsunami fragility analysis could be an efficient tool within a probabilistic risk assessment framework (Koshimura et al. 2009; Attary et al. 2017; Medina et al. 2019). However, studies regarding fragility analysis of bridges subjected to tsunami hazards are still limited. Akiyama et al. (2013) developed tsunami fragility curves for a specific Tsutanigawa concrete bridge. Shoji and Moriyama (2007) constructed empirical tsunami fragility curves of the bridges damaged in the 2004 Indian Ocean tsunami event. Based on an expert opinion survey approach, the Hazus (FEMA 2013) proposed fragility curves for highway bridges subjected to tsunami hazards.

[1]Assistant Professor, College of Civil Engineering, Nanjing Tech Univ., Nanjing 211816, China; formerly, Ph.D. Candidate, Key Laboratory of Concrete and Prestressed Concrete Structures of the Ministry of Education, Southeast Univ., Nanjing 210096, China.

[2]Associate professor, Key Laboratory of Concrete and Prestressed Concrete Structures of the Ministry of Education, Southeast Univ., Nanjing 210096, China. ORCID: https://orcid.org/0000-0003-3691-6128.

[3]Professor, Key Laboratory of Concrete and Prestressed Concrete Structures of the Ministry of Education, Southeast Univ., Nanjing 210096, China (corresponding author). ORCID: https://orcid.org/0000-0002-9405-3757. Email: g.wu@seu.edu.cn

Note. This manuscript was submitted on December 6, 2019; approved on December 21, 2020; published online on March 24, 2021. Discussion period open until August 24, 2021; separate discussions must be submitted for individual papers. This paper is part of the ***Journal of Bridge Engineering***, © ASCE, ISSN 1084-0702.

The inundation depth of the flow is used as the tsunami intensity measure, and the flow velocity is considered only with a modification factor on the fragility function. The Hazus tsunami fragility curves also do not differentiate bridge classes (Gidaris et al. 2017). Thus, it can be seen that more research efforts are required in order to better understand the vulnerability of the coastal bridges subjected to tsunami hazards.

On the other hand, bridge aging and degradation with time will adversely affect bridge performance. Approximately 40% of the bridges in the Unite Sates have serviced for more than 50 years (FHWA 2019). Aging bridges can also be seen in other regions of the world. Chloride-induced corrosion is considered as a major factor of aging and degradation for RC bridges, especially for bridges located in coastal regions (Alipour et al. 2011). The corrosion of steel reinforcements reduces the effective sectional area and material properties of steel reinforcements. Corrosion products can also induce cracking as well as spalling of cover concrete. Because of corrosion over time, the structural performance degrades gradually and the degradation of structural performance makes the bridge more susceptible when subjected to other nature hazards. The joint effects of aging and other nature hazards on bridge performance have gained significant research attention (Ranjkesh et al. 2019; Akiyama et al. 2020), with much about the assessment of combined effects of earthquake and corrosion on RC bridges (Biondini et al. 2014; Cui et al. 2018; Deng et al. 2018). Researches regarding seismic performance assessment of bridges considering corrosion effects indicate that corrosion can reduce the bridges' seismic capacity (Ghosh and Sood 2016; Cheng et al. 2019) and increase the fragility of bridges under earthquakes (Ghosh and Padgett 2010; Guo et al. 2015). The life-cycle seismic reliability (Akiyama et al. 2011; Yanweerasak et al. 2018) and resilience of bridges (Vishwanath and Benerjee 2019) have also been found to be adversely affected by corrosion. These researches highlight the potential importance of considering aging and degradation effects on performance assessment of bridges when subjected to other nature hazards. However, research effort regarding life-cycle performance assessment of coastal bridges under tsunami hazard simultaneously considering aging effects is still quite limited.

Addressing the present research drawbacks, in this work the collapse fragility analysis is conducted to investigate the life-cycle performance of aging coastal RC bridges subjected to tsunami hazards. The joint effects of time-dependent aging and tsunami hazards are simultaneously considered toward more realistic performance assessment. The chloride-induced corrosion is considered as the deterioration mechanism and, via corrosion modeling, the time-dependent corrosion levels of transverse and longitudinal reinforcements are obtained. The effects of corrosion are considered through the appropriate modification of material properties, including steel reinforcements and concrete. Shear-capacity deterioration of the bridge columns due to transverse reinforcement corrosion is also accounted for. The Latin hypercube sampling (LHS) method is used to consider uncertainties from materials in developing numerical bridge models. Nonlinear tsunami pushover analysis is used to investigate the bridge damage under tsunami loading. The tsunami collapse fragility curves are calculated assuming a lognormal distribution and, with a quadratic model for the median and standard deviation of tsunami intensity, the time-dependent tsunami collapse fragility curves are obtained.

A three-span, two-column bent RC bridge is selected to conduct the collapse fragility analysis within 100 years. The effects of flow inundation depth and time-dependent aging on bridge column failure modes under tsunami loadings are investigated. The time-dependent tsunami collapse fragility curves of the bridges are derived and factors influencing failure probability are also investigated and discussed.

Time-Dependent Deterioration Modeling

Chloride-Induced Corrosion Modeling

For coastal RC bridges, chloride-induced corrosion is generally considered as one of the major deterioration mechanisms due to the natural chlorine in the air and sea water. In order to define the corrosion levels of the bridge, the corrosion modeling method proposed by Choe et al. (2009) is adopted in the current work. Generally, the corrosion process can be divided in two phases: initiation phase and propagation phase.

For the initiation phase, the corrosion initiation time T_0 (year) can be calculated following Choe et al. (2009) as

$$T_0 = X_I \left\{ \frac{x_c^2}{4k_e k_t k_c D_0 t_0^n} \left[erf^{-1}\left(\frac{C_s - C_{cr}}{C_s} \right) \right]^{-2} \right\}^{1/(1-n)} \quad (1)$$

where X_I = model uncertainty factor and is taken as 1.0; k_e = environment factor; k_t = test factor; k_c = curing factor; D_0 = reference diffusion coefficient; t_0 = reference period; n = age factor; C_s = equilibrium chloride concentration at the concrete surface; C_{cr} = critical chloride concentration; $erf^{-1}(\cdot)$ = Gaussian error function; and x_c = concrete depth, and in this work, this value is considered differently for transverse and longitudinal reinforcement due to their different embedment depths.

After corrosion initiation, the corrosion enters into the propagation phase where the steel reinforcements begin to be corroded. Assuming uniform corrosion condition, the corrosion rate over time is calculated as (Vu and Stewart 2000)

$$r_{cr}(t) = \frac{32.13(1 - w/c)^{-1.64}}{x_c}(t - T_0)^{-0.29} \quad (2)$$

where $r_{cr}(t)$ = corrosion rate at time t, w/c = water-to-cement ratio.

Then the time-dependent erosion depth $e_{\text{cor}}(t)$ is calculated as (Choe et al. 2009)

$$e_{\text{cor}}(t) = 0.0116 \int_{T_0}^{t} r_{cr}(t)dt = \frac{0.5254(1 - w/c)^{-1.64}}{x_c}(t - T_0)^{0.71} \quad (3)$$

The diameter of corroded steel reinforcement at time t is evaluated as

$$d_{\text{cor}}(t) = d_0 - 2e_{\text{cor}}(t) \quad (4)$$

where $d_{\text{cor}}(t)$ and d_0 = diameter of the corroded and uncorroded steel reinforcements, respectively. The time-dependent corrosion level of steel reinforcement is calculated as

$$X_{\text{cor}}(t) = \frac{d_0^2 - d_{\text{cor}}^2(t)}{d_0^2} \times 100\% \quad (5)$$

where $X_{\text{cor}}(t)$ = corrosion level that is determined in terms of percentage of mass loss of the steel reinforcement.

Corrosion Effects on Material Properties

Generally, corrosion will induce the deterioration of yield strength as well as elastic modulus of the steel reinforcements. The reduced yield strength and elastic modulus of steel reinforcement are evaluated by

the empirical formulae proposed by Du et al. (2005a, b)

$$f_{y,\text{cor}} = f_{y0}(1 - 0.005X_{\text{cor}}) \tag{6}$$

$$E_{y,\text{cor}} = E_{y0}(1 - 0.01X_{\text{cor}}) \tag{7}$$

where $f_{y,\text{cor}}$ and f_{y0} = yield strength of corroded and uncorroded steel reinforcements, respectively; $E_{y,\text{cor}}$ and E_{y0} = elastic modulus of corroded and uncorroded steel reinforcements, respectively; and X_{cor} = corrosion level.

In addition to the reduced material properties of steel reinforcement, this study also considers the reduced confining effect on core concrete due to the degraded properties of transverse reinforcement. The confined concrete model proposed by Mander et al. (1988) is adopted to calculate the core concrete strength:

$$f_{cc} = f_c\left(2.254\sqrt{1 + \frac{7.94f_{le}}{f_c}} - 2\frac{f_{le}}{f_c} - 1.254\right) \tag{8}$$

where f_{cc} = confined core concrete strength; f_c = unconfined cover concrete strength; f_{le} = effective confining pressure, and the evaluation of this parameter can be referred to (Mander et al. 1988).

The ultimate strain ε_{cu} of the confined core concrete is calculated as

$$\varepsilon_{cu} = 0.004 + \frac{1.4\rho_{vt}f_{yt,\text{cor}}\varepsilon_{su}}{f_{cc}} \tag{9}$$

where ρ_{vt} = volumetric ratio of transverse reinforcement; and $f_{yt,\text{cor}}$ and ε_{su} = yield strength and ultimate strain of corroded transverse reinforcement, respectively.

Corrosion Effects on Shear Capacity of Columns

Due to the smaller diameter and closer distance to corrosive environment, the transverse reinforcement can be corroded more severely compared with longitudinal reinforcement, and lead to more significant shear strength deterioration, causing a change of column failure mode from flexure to flexure–shear (Vu and Li 2018a). As demonstrated by some recent experimental studies (Vu and Li 2018a), corroded concrete columns could fail in shear under lateral loadings although they were initially ductile-designed. This work also considers the shear-capacity deterioration because of corrosion effects in order to account for the possible shear failure of bridge columns under tsunami loadings.

The shear strength model developed by Vu and Li (2018b) is adopted to evaluate the reduced shear strength of the corroded bridge column:

$$V_n = V_c + V_s \tag{10}$$

where V_n = total shear strength of concrete column, V_c = shear strength contribution of concrete, and V_s = shear strength contribution of transverse reinforcement. Due to the degraded material properties of transverse reinforcement, the shear strength contributed by transverse reinforcement will be reduced and is evaluated as (Vu and Li 2018b)

$$V_s = \frac{A_{st,\text{cor}}f_{yt,\text{cor}}d}{s} \tag{11}$$

$$A_{st,\text{cor}} = (1 - X_{t,\text{cor}})A_{st} \tag{12}$$

where $A_{st,\text{cor}}$ and A_{st} = total cross-sectional area of corroded and uncorroded transverse reinforcement, respectively; $f_{yt,\text{cor}}$ = yield strength of corroded transverse reinforcement and is evaluated by Eq. (6); s = transverse reinforcement spacing; d = effective depth of column section; and $X_{t,\text{cor}}$ = corrosion level of transverse reinforcement.

Because of the cracks in cover concrete caused by the corrosion products, the strength of cover concrete will degrade and then the shear strength contributed by concrete will also degrade and is evaluated as (Vu and Li 2018b)

$$V_c = \left[\frac{0.5\sqrt{f_c}}{a/d}\sqrt{1 + \frac{P}{0.5\sqrt{f_c}(A_{\text{core}} + \sqrt{\zeta}A_{\text{cover}})}}\right] \cdot 0.8(A_{\text{core}} + \sqrt{\zeta}A_{\text{cover}}) \tag{13}$$

where A_{core} and A_{cover} = area of core concrete and cover concrete, respectively; a = shear span of the column; P = axial load; and ζ = softening coefficient of cover concrete that is evaluated as (Hsu and Mo 2010)

$$\zeta = \frac{0.9}{\sqrt{1 + 600\varepsilon_{cr}}} \tag{14}$$

$$\varepsilon_{cr} = \frac{w_{cr}}{b_0} \tag{15}$$

where ε_{cr} = tensile strain caused by the cracks of the cover concrete, b_0 = column section circumference, and w_{cr} = total crack width. In this work, an empirical relationship between total crack width and transverse reinforcement corrosion level is used to evaluate the total crack width (Vu and Li 2018b)

$$X_{t,\text{cor}} = 21.91w_{cr}(\text{mm}) + 5.34 \tag{16}$$

Prototype Bridge and Finite Element Modeling

Prototype Bridge

A three-span RC box-girder bridge is selected in this work to evaluate its life-cycle performance under tsunami hazards. This bridge represents typical bridge configuration in California (Mangalathu and Jeon 2019). As shown in Fig. 1, the two end spans of the bridge are 25 m in length and the intermediate span is 36 m in length. The bridge has two two-column bents and each bent has two concrete columns with 6.5 m in height and 1.22 m in section width, as shown in Fig. 2. The column has 26 longitudinal reinforcements with a diameter of 32 mm. The column is assumed to have a pinned connection at the column base that is commonly used for multicolumn bent bridges in California (Jeon et al. 2019). The transverse reinforcement is 16 mm in diameter and 100 mm in center-to-center spacing. The top width of the box-girder is 17 m and the bottom width is 14 m, and the height is 2.6 m. The ends of the girder are supported by two integral diaphragm abutments on six concrete piles.

Finite Element Modeling of the Bridge

Analytical 3D finite element models of the bridge are developed in OpenSees (Mazzoni et al. 2005). As shown in Fig. 1, the deck is modelled with elastic beam–column elements in the longitudinal

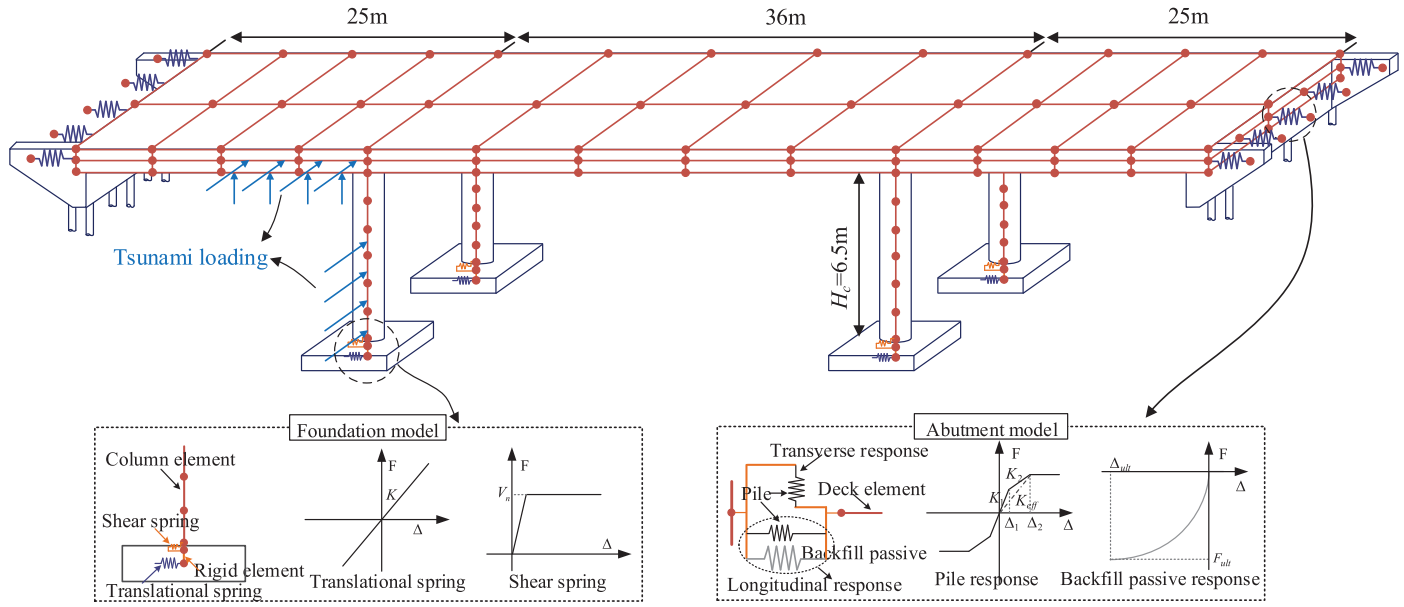

Fig. 1. Overall layout and numerical modeling of the bridge.

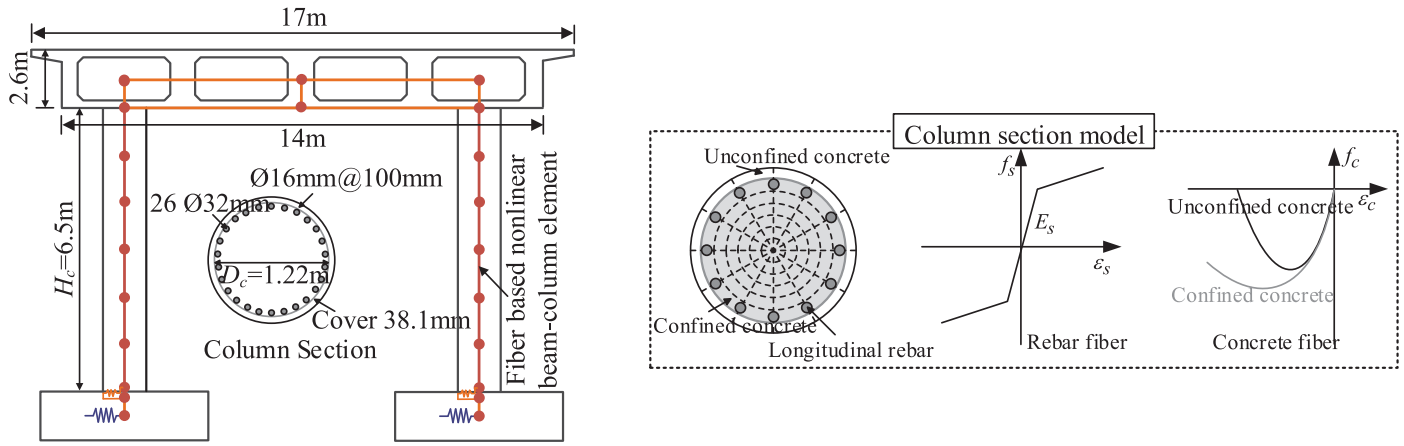

Fig. 2. Two-column bent information and numerical modeling of the bent.

direction; rigid elements are adopted to model the deck in the transversal direction. Several zero-length spring elements are adopted for modeling the abutments. The longitudinal response of the abutment is considered to include passive reaction and active reaction. The passive reaction is assumed to be provided by backfill and piles, and active reaction is assumed to be provided by piles. The transversal response is assumed to be provided by piles only. The passive response of the abutment backfill is modeled with the hyperbolic soil model proposed by Shamsabadi et al. (2010), and the trilinear spring model is used for modeling piles response (Choi et al. 2004). The foundation is modeled with zero-length translational and rotational linear spring elements and the stiffness of these spring elements are provided in Table 1. As shown in Fig. 2, columns are modeled with fiber-based nonlinear beam–column elements assigned with a fiber section, and the steel fibers are modeled using Steel 02 uniaxial material model and concrete fibers are modeled using the Concrete 01 uniaxial material model.

To account for the possible shear failure of the bridge column under tsunami loadings, a zero-length shear spring element is added at the end of the column base to account for the shear response. Due to the force-controlled failure mechanism of structures under tsunami loading (Scott and Mason 2017), the bridge is considered as failed once the shear capacity of the column is attained. For this reason, the shear behavior is assumed to be elastic–perfectly plastic for numerical modeling convenience. A large value of initial shear elastic stiffness is assumed because the shear deformation of concrete column is generally rather small compared with flexural deformation.

The uncertainties in developing bridge models are also considered. Table 1 lists the sources of uncertainties and their distribution functions and parameters. In this work, the LHS method is adopted to generate random variables in developing the numerical bridge models.

Time-Dependent Collapse Fragility Analysis

Fragility Function

In this work, the life-cycle performance of RC bridges is evaluated by conducting collapse fragility analysis under tsunami loading. The collapse fragility curves are developed to evaluate the failure

Table 1. Uncertainty parameters and the probability distribution

Random variable	Type	Parameters	
		Mean	Standard deviation
Concrete compressive strength, f_c (MPa)	N	29.03	3.59 (Mangalathu 2017)
Concrete strain at f_c, ε_c	N	0.0022	0.0004 (Barbato et al. 2014)
Rebar yield strength, f_y (MPa)	LN	465	37.30 (Mangalathu 2017)
Strain–hardening ratio, b	N	0.005	0.00075 (Barbato et al. 2014)
Pile stiffness, K_{eff} (kN/mm)	LN	14	0.3 (Ramanathan 2012)
Translational stiffness, K_t (kN/mm)	LN	175.1	0.44 (Mangalathu and Jeon 2019)
Transverse rotational stiffness, K_r (GN-m/rad)	LN	1.36	0.28 (Mangalathu and Jeon 2019)

probability of the bridge at given tsunami hazard levels. Because both of the flow velocity and inundation depth can affect bridge responses under tsunami loading, in this study a vector intensity measure is adopted in order to better describe the tsunami hazard and predict the bridge responses. The flow velocity u and inundation depth h are taken as the intensity measures. Assuming a lognormal distribution (Gidaris et al. 2017) and for a given inundation depth h, the cumulative collapse failure probability is calculated as

$$P(u, h) = \Phi\left(\frac{\ln u - \ln m_{u(h)}}{\zeta_{u(h)}}\right) \tag{17}$$

where $P(u, h)$ = collapse probability of the bridge under a tsunami with flow velocity u and inundation depth h; and $m_{u(h)}$ and $\zeta_{u(h)}$ = median and log-standard deviation of the flow velocity u causing bridge collapse at inundation depth h.

Collapse Fragility Function Considering Time-Dependent Aging Effects

The previous collapse fragility curves are developed for pristine bridges without considering aging effects; however, as described previously, coastal bridges may suffer from corrosion induced damage. The corrosion is time-dependent and, hence, a time-dependent fragility function is adopted to evaluate the effects of corrosion on the collapse failure probability of RC bridges under tsunami loading. The time-dependent collapse fragility function is expressed as

$$P(u, h, t) = \Phi\left(\frac{\ln u - \ln m_{u(h)}(t)}{\zeta_{u(h)}(t)}\right) \tag{18}$$

where $P(u, h, t)$ = collapse probability of the bridge under a tsunami with flow velocity u and inundation depth h at a given year t; $m_{u(h)}(t)$ and $\zeta_{u(h)}(t)$ = function of time; and $m_{u(h)}(t)$ and $\zeta_{u(h)}(t)$ are calculated at several selected years and then a quadratic model is used to fit and predict $m_{u(h)}(t)$ and $\zeta_{u(h)}(t)$ at different target years (Ghosh and Padgett 2010)

$$\psi(t) = p_1 t^2 + p_2 t + p_3 \tag{19}$$

where $\psi(t)$ = either $m_{u(h)}(t)$ or $\zeta_{u(h)}(t)$ at a given year t, and p_1, p_2, and p_3 = quadratic coefficients.

With the obtained quadratic coefficients for $m_{u(h)}(t)$ and $\zeta_{u(h)}(t)$, the time-dependent collapse fragility function is expressed as

$$P(u, h, t) = \Phi\left(\frac{\ln u - \ln (p_{1-m}t^2 + p_{2-m}t + p_{3-m})}{p_{1-\zeta}t^2 + p_{2-\zeta}t + p_{3-\zeta}}\right) \tag{20}$$

where p_{1-m}, p_{2-m}, and p_{3-m} denote quadratic coefficients for the median $m_{u(h)}(t)$; $p_{1-\zeta}$, $p_{2-\zeta}$ and $p_{3-\zeta}$ denote quadratic coefficients for the standard deviation $\zeta_{u(h)}(t)$.

Tsunami Pushover Analysis (TPO)

Tsunami Loading

The time-dependent collapse fragility curves are developed using nonlinear static tsunami pushover analysis. First, the tsunami loading is evaluated to define the force applied on the bridge system at given inundation depth and flow velocity. Generally, tsunami loading imposed on bridge systems can be classified into two cases. As shown in Fig. 3, the first case is that the flow depth is below the deck ($h \le H_c$) and the second case is that the flow depth reaches to the deck ($h > H_c$). When the flow depth is below the deck, tsunami flow loading will impose on bridge columns only. Based on the experimental and numerical results (Arnason et al. 2009; Asadollahi et al. 2019), the maximum tsunami force imposed on a column can be evaluated as the total hydrodynamic force. Thus following Arnason et al. (2009) and FEMA (2012), the total tsunami force F_{Col} imposed on bridge column is evaluated as

$$F_{\text{Col}} = 0.5\rho_s C_D B h u^2 \tag{21}$$

where h = inundation depth, u = flow velocity that is assumed to be uniformly distributed along the inundation depth, B = breadth of the structure in the plane perpendicular to the flow, ρ_s = fluid density, and C_D = drag coefficient.

When the flow depth reaches to the deck, tsunami flow will simultaneously induce horizontal and vertical loads on the bridge deck. The evaluation of the maximum horizontal tsunami force on the deck is relatively complex and many factors, such as deck section shape, bridge skewness, and connection flexibilities to substructures, could affect the magnitude of the maximum horizontal tsunami force. In the present study, the method proposed by Azadbakht and Yim (2016) is adopted for evaluating the maximum horizontal force imposed on the bridge deck

$$F_H = F_{Hs} + F_{Hd} = 0.5\rho_s g h_d^2 + 0.5\rho_s C_D h_d u^2 \quad (h_d \le L_r) \tag{22}$$

where F_H = total maximum horizontal tsunami force per unit length; F_{Hs} = horizontal hydrostatic force that is flow velocity independent; F_{Hd} = horizontal hydrodynamic force that is flow velocity dependent; g = gravity acceleration; h_d = flow depth on the deck ($h_d = h - H_c$); and L_r = depth of bridge deck, as shown in Fig. 3.

Following Azadbakht and Yim (2016), the tsunami flow can induce uplift force on the bridge deck if the flow depth reaches to the deck, and can induce downward vertical force if the flow depth is higher than the top of the bridge deck. The present study only

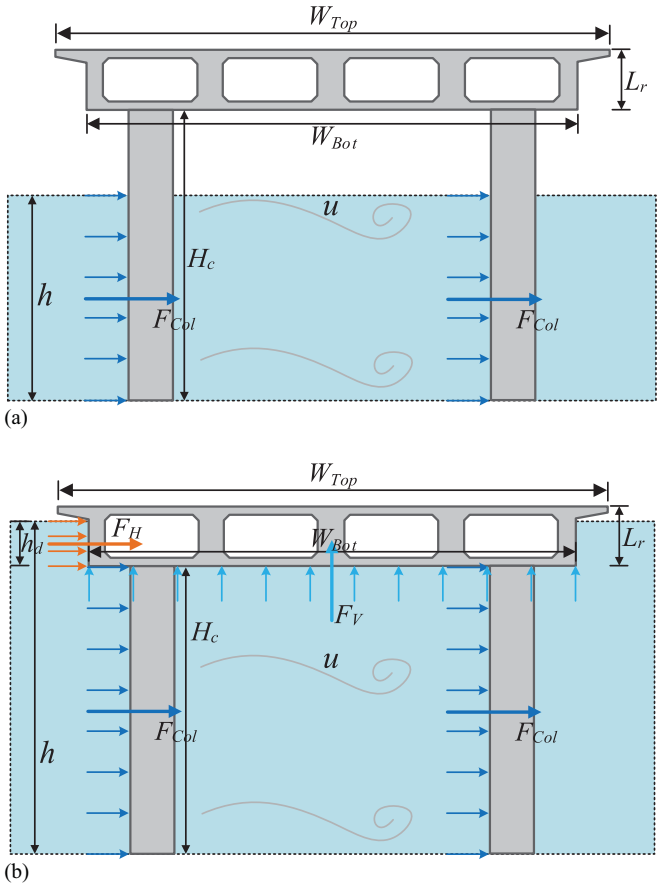

Fig. 3. Tsunami loading scenarios considered for bridge: (a) flow is below the deck ($h \le H_c$); and (b) flow reaches to the deck ($h > H_c$).

considers the situations in which the flow depth is below the top of the deck; thus, only the maximum uplift force is considered and is assumed to occur simultaneously with the maximum horizontal force. Based on Azadbakht and Yim (2016), the maximum uplift force F_V can be evaluated as

$$F_V = C_{UP}(F_{Vb} + F_{Vl}) = C_{UP}(\rho_s g V + 0.5 C_l \rho_s W u^2) \quad (23)$$

where F_{Vb} = buoyancy force that is flow velocity independent and F_{Vl} = lift force (vertical hydrodynamic force) that is flow velocity dependent, V = volume of the displaced water, W = width of the bridge deck, C_{UP} = empirical uplift force coefficient and is taken as 0.77, and C_l = lift coefficient and is taken as $0.5C_D$ for simplicity.

To consider the uncertainties in tsunami loading, the fluid density ρ_s and the drag coefficient C_D are considered as random variables in this study. The probability distribution functions and the defining parameters of these two random variables are given in Table 2.

Nonlinear Pushover Analysis

During the nonlinear static tsunami pushover analysis, the inundation depth h is firstly prespecified and then the flow velocity u is incrementally increased. As the hydrodynamic forces are flow velocity dependent and, thus, the hydrodynamic forces will be applied on the bridge column or/and the deck (in the case where the flow height reaches to the deck) as uniformly distributed pressure increased with the flow velocity. Meanwhile, when the flow height reaches to the deck, the horizontal hydrostatic force and vertical buoyancy force will be applied on the deck. The displacement-controlled nonlinear pushover analysis with the Krylov–Newton algorithm method is used in order to capture the descending branch of the pushover curve (Feng et al. 2019). However, as the failure of structures under tsunami loading is typically force controlled rather than displacement controlled, only the maximum tsunami force achieved at or below a particular drift limit is used for fragility analysis. In this study, the collapse drift limit of the bridge column is 5% (Jeon et al. 2016; Mangalathu et al. 2018), which is usually used as the collapse limit for bridge columns under seismic loading. The complete failure limit state definition of integral diaphragm abutments is yet not clear and the complete failure of abutment has been seldom considered in fragility analysis of bridges under tsunami or seismic loadings (Shoji and Moriyama 2007; Jeon et al. 2019; Mangalathu and Jeon 2019); thus, the complete failure of abutments under tsunami loadings is not considered in the present study.

Table 2. Random variables of tsunami loading

Random variable	Type	Distribution
Drag coefficient, C_D	Uniform	(1.25–3) (Fujima et al. 2009)
Fluid density, ρ_s (kg/m^3)	Uniform	(1,000–1,200) (Alam et al. 2018)

Results and Discussion

Tsunami Pushover Response

With the assumed exposure condition (refer to the Appendix) of the bridge, the corrosion levels of the reinforcements can be obtained through the corrosion modeling method described previously. Fig. 4 presents the time-dependent corrosion levels of transverse and longitudinal reinforcements of the bridge columns. The corrosion initiation time is 7.2 years for transverse reinforcements, and the corrosion initiation time increases to 21.8 years for longitudinal reinforcements due to their thicker embedded depth.

The time-dependent column tsunami pushover response is discussed first. Fig. 5 depicts the average applied horizontal hydrodynamic force on the bridge column versus column drift ratio curves at time 0 year (i.e., pristine bridge). Seven inundation depth cases are investigated, with four cases below the deck (3.0–6.0 m) and three cases above the deck (7.0–9.1 m). For each inundation depth and a given investigated year, 100 bridge samples are generated via the LHS method with the random material properties listed in Table 1.

As presented in Fig. 5, the inundation depth has significant effects on the column TPO response. At low inundation depth, that is, 3.0 and 4.0 m, the column generally fails in shear mode. It is mainly because the applied uniformly distributed pressure on the columns at low inundation depth will result in a low shear span to depth ratio. While with the increasing inundation depth, the failure mode of the column shift to flexure and the maximum horizontal hydrodynamic force decreases. For inundation depths reaching to the deck, a significant reduction of horizontal hydrodynamic force is observed. Due to the jump of breadth perpendicular to the flow and large horizontal tsunami forces imposed on the deck, the required flow velocity causing bridge failure significantly decreases and hence, the horizontal hydrodynamic force applied on the bridge column component significantly decreases.

Detailed TPO responses of bridge columns are shown in Fig. 6 for the 4.0 and 7.8 m inundation depth cases, which represent typical shear failure and flexure failure modes. As can be seen from Fig. 6(a), for the 4.0 m inundation depth case, the columns generally fail in shear modes at the 0 and 50 year marks and, when time

increases the maximum horizontal hydrodynamic force decreases due to the reduced shear capacity of columns. For the 7.8 m inundation depth case, as shown in Fig. 6(b), bridge columns all fail in flexure mode. However, although in many cases the maximum horizontal hydrodynamic force is achieved below the 5% collapse drift limit, there are some cases in which the maximum horizontal hydrodynamic force occurs after the 5% collapse drift limit. It is mainly because the tsunami flow could induce large vertical uplift force on the bridge deck for the 7.8 m inundation depth case, and the axial compression force of the column is significantly reduced, thus the pushover curves could still experience hardening behavior even after the 5% collapse drift limit. However, only the horizontal hydrodynamic force corresponding to 5% collapse drift limit will be used for collapse fragility analysis.

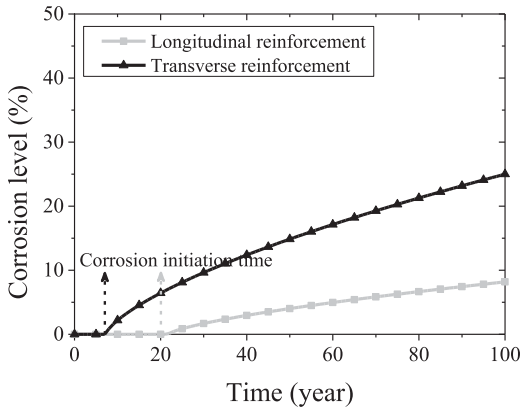

Fig. 4. Time-dependent corrosion levels of reinforcements of bridges columns.

The effect of shear capacity degradation on failure modes of bridges columns is also investigated. Fig. 7 shows the time-dependent shear capacity of the bridge column. It can be seen that because of the corrosion of the transverse reinforcements, the shear capacity decreases over time. The mean shear capacity at year 0 is 2,371.1 kN, whereas it will decrease to 1,981.3 kN at year 50, with a reduction of 16.4%. The deterioration of shear capacity can change the failure mode of the bridge column. Fig. 8 compares the columns TPO responses for 6.0 m inundation depth at the 0 and 50 year marks. It can be seen that most of the columns fail in flexure at year 0, however more columns will experience shear failure mode at year 50 under tsunami loading. Thus, more attention should be paid in shear capacity deterioration evaluation for life-cycle performance assessment of RC bridges under tsunami loading.

Fig. 9 compares the average TPO responses of columns at different investigated years. Because the TPO response for other

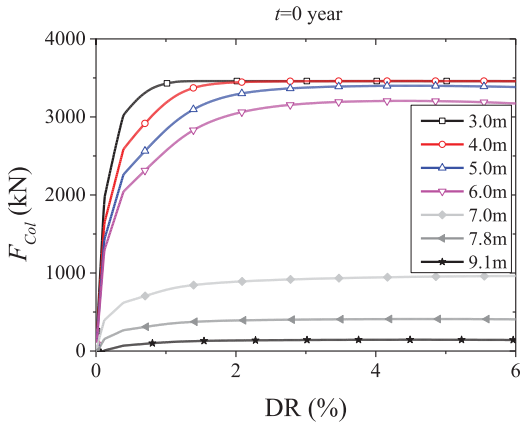

Fig. 5. Average tsunami push-over responses of bridge columns at time 0 year for various inundation depths.

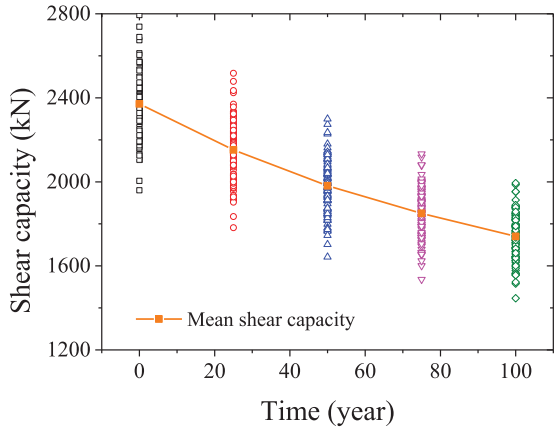

Fig. 7. Time-dependent shear capacity of bridge columns.

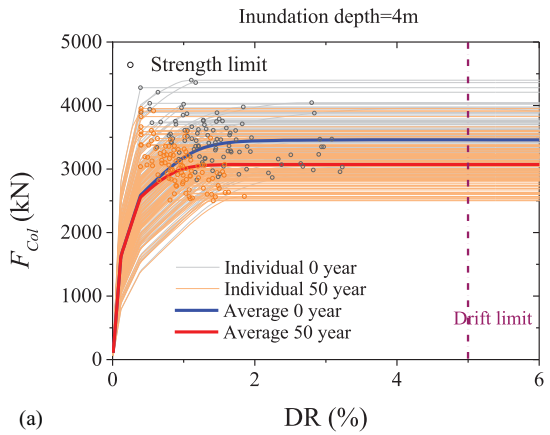

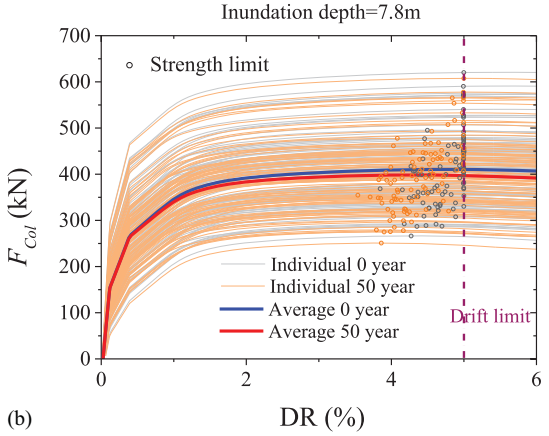

Fig. 6. The individual and average tsunami push-over curves of bridge columns at time 0 and 50 year: (a) 4.0 m inundation depth; and (b) 7.8 m inundation depth.

J. Bridge Eng., 2021, 26(6): 04021025

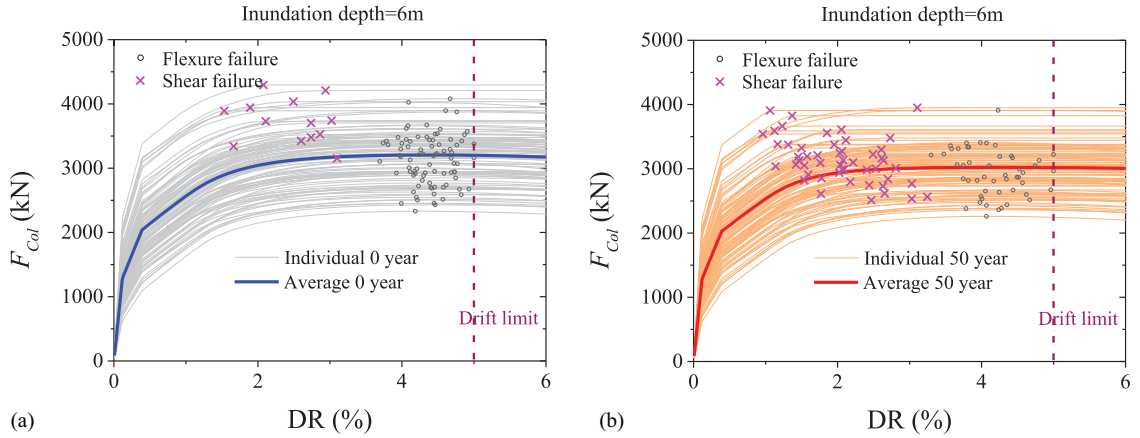

Fig. 8. The individual and average tsunami push-over curves of bridge columns for 6.0 m inundation depth: (a) at time 0 year; and (b) at time 50 year.

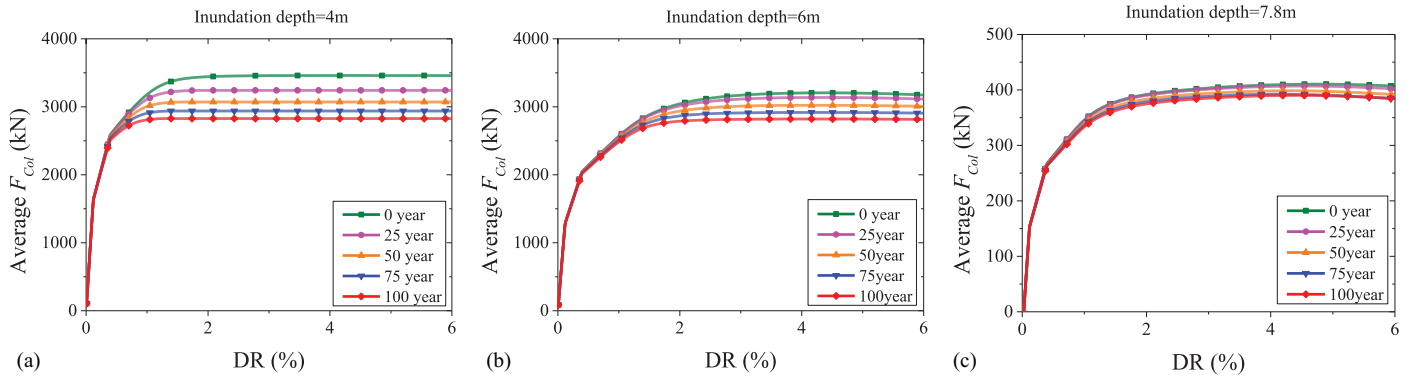

Fig. 9. The average tsunami push-over curves of bridge columns at different investigated year for variant inundation depths: (a) 4.0 m; (b) 6.0 m; and (c) 7.8 m.

inundation depths exhibit a similar trend over time, only 4.0, 6.0, and 7.8 m inundation depths are shown in this figure. It can be observed from Fig. 9 that corrosion can affect the maximum tsunami capacity of bridge columns. The maximum tsunami capacity decreases over time, especially for low inundation depths, that is,. 4.0 m, where columns fail in shear, due to the higher corrosion levels of transverse reinforcement. For higher inundation depths, that is, 7.8 m, where the column fails in flexure, the maximum tsunami capacity also decreases over time due to corrosion effects. However, the effect of corrosion is slight due to the lower corrosion levels of longitudinal reinforcement for this bridge and environment condition considered in this study.

Collapse Fragility Results

Based on the TPO responses of the bridge, the required horizontal hydrodynamic force imposed on the column causing bridge collapse at variant inundation depths can be obtained. Then based on Monte Carlo simulation, the required flow velocity causing bridge collapse at variant inundation depths is obtained. The collapse fragility curves of the bridge can be calculated based on Eq. (17). Fig. 10 illustrates the collapse fragility curves for variant inundation depths at year 0. It can be seen that the inundation depth can significantly affect the collapse fragility of the bridge. A clear jump of failure probability for inundation depth from below to above the deck can be observed. The median collapse flow velocity

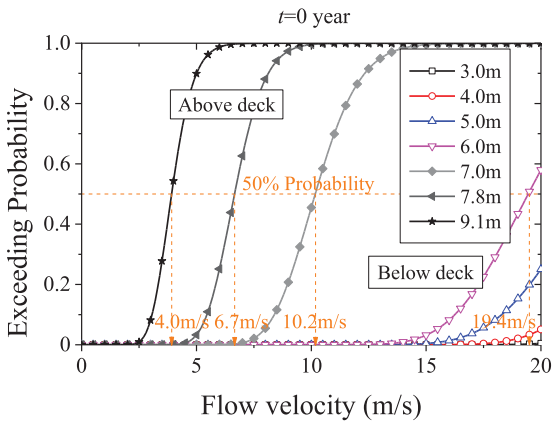

Fig. 10. Collapse fragility curves for variant inundation depths at time 0 year.

is larger than 19.4 m/s for inundation depth below the deck, while the median collapse flow velocity will decrease to 10.2, 6.7, and 4.0 m/s for 7.0, 7.8, and 9.1 m inundation depth flow, respectively. Although the median collapse flow velocity for inundation depth below the deck is very large and is unlikely to occur, the median collapse flow velocity for the flow with a height reaches to the deck can be within the range for recent tsunami events

(Fritz et al. 2012; Yeh et al. 2013). Thus, the bridge has a high failure probability if it is subjected to a tsunami hard with a flow height reaching to the deck.

After obtaining the median and standard deviation of the flow velocity for different investigated years, the time-dependent collapse fragility curves of the bridge can be calculated based on the Eqs. (19) and (20). Fig. 11 presents fitting results for the 7.8 m inundation depth case based on Eq. (19). It can be seen that the median flow velocity slightly decreases over time, which shows the reduced tsunami capacity of the bridge due to corrosion effects.

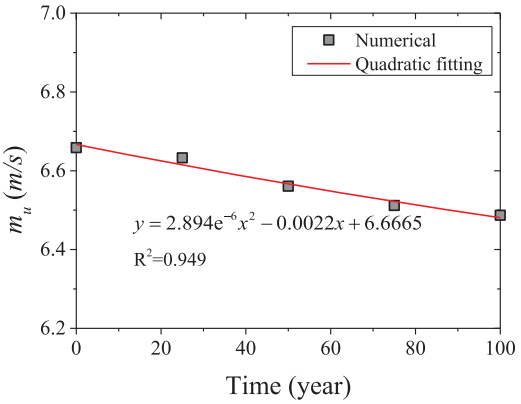

Fig. 11. Quadratic fitting results of median flow velocity for 7.8 m inundation depth.

Fig. 12 depicts the parameterized time-dependent collapse fragility surfaces of the bridge, calculated based on Eqs. (19) and (20). It can be seen that failure probability increases with the flow velocity, especially for high inundation depth cases where the bridge is more vulnerable under tsunami loading. The failure probability gradually increases over time, especially for low inundation depth due to the shear failure mode of the columns and the significant deterioration of shear capacity of the columns due to corrosion.

Fig. 13 depicts the interaction diagram of aging time and flow velocity at 50% exceeding probability for variant inundation depths. Fig. 13 shows that the flow velocity causing bridge collapse is significantly affected by the inundation depth. As inundation depth increases, the required flow velocity significantly decreases. However, the flow velocity shows a decreasing trend over time for low inundation depths, but does not significantly decrease for higher inundation depths. It is mainly due to the lower corrosion levels of longitudinal reinforcement in this case.

The time-dependent collapse fragility curves and time-dependent failure probability difference are shown in Figs. 14–17 for four inundation depth cases. Figs. 14 and 15 present the collapse failure probability and failure probability difference of the bridge subjected to 5.0 and 6.0 m inundation depth flow, respectively. It can be seen from Figs. 14(a) and 15(a) that the failure probability increases over time. Figs. 14(b) and 15(b) show that, due to corrosion effects, the failure probability difference increases over time. The maximum probability difference of the bridge at year 0 and 100 could be 22% when subjected to 6.0 m inundation depth flow with a velocity of 18.5 m/s. However, the median collapse flow velocity is still very large within 100 years. As shown

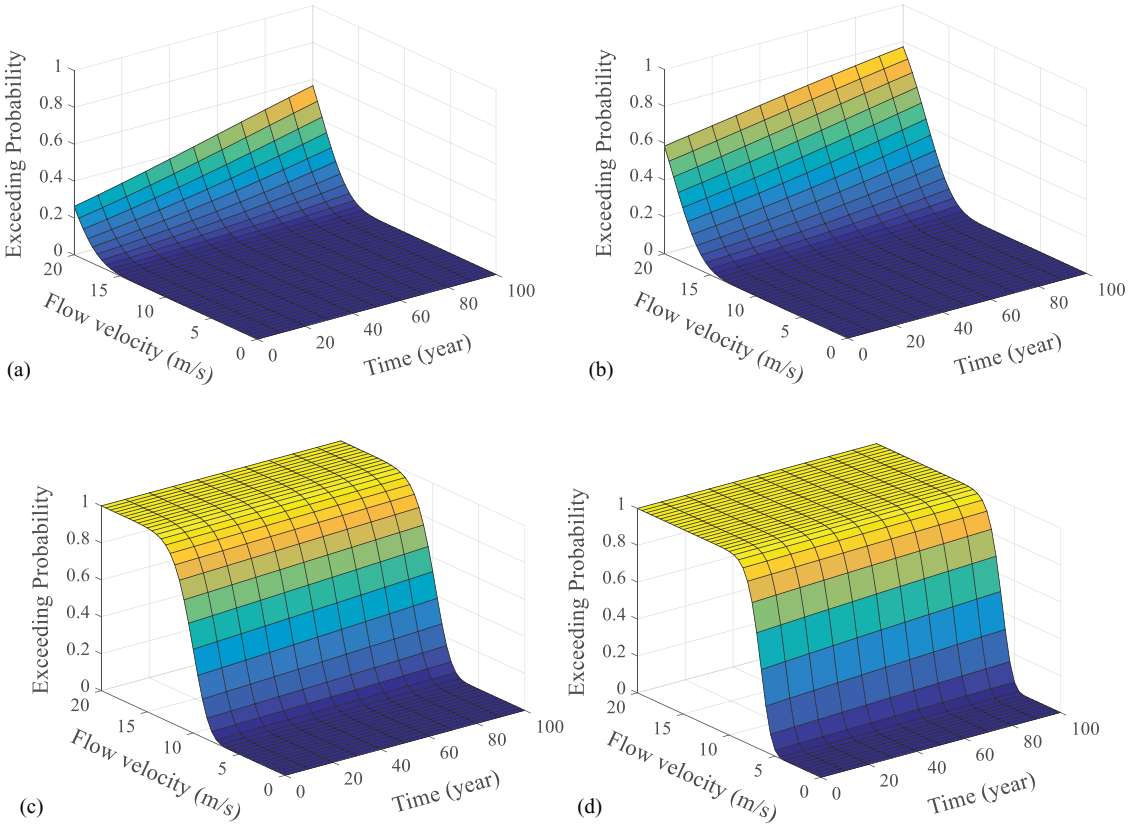

Fig. 12. Parameterized time-dependent collapse fragility surfaces: (a) 5.0 m inundation depth; (b) 6.0 m inundation depth; (c) 7.0 m inundation depth; and (d) 7.8 m inundation depth.

in Fig. 14(a), for 5.0 m inundation depth flow, the median collapse flow velocity is still larger than 19 m/s at 100 year. Fig. 15(a) shows that the median collapse flow velocity is 19.4 m/s at year 0 and 17.9 m/s at year 100 for 6.0 m inundation depth flow. These large flow velocity values are unlikely to occur for tsunami events which indicates that the bridge has a high tsunami security if the depth of the flow is below the deck.

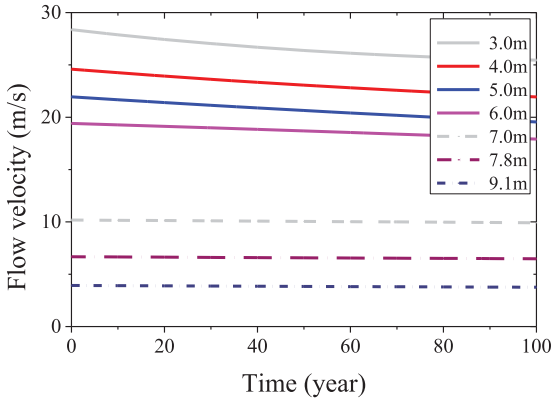

Fig. 13. Interaction diagrams of aging time and flow velocity at 50% exceeding probability.

Figs. 16 and 17 present the collapse failure probability and failure probability difference of the bridge subjected to 7.0 and 7.8 m inundation depth flow which reaches to the bridge deck. It can be seen that the failure probability generally slightly increases over time and the failure probability difference also increases over time. As shown in Fig. 16(b), the maximum probability difference of the bridge at year 0 and 100 could be 6.8% when subjected to 7.0 m inundation depth flow with a velocity of 10.0 m/s. Fig. 17(b) shows that, for 7.8 m inundation depth flow, the maximum probability difference of the bridge at year 0 and 100 could be 7.2% at 6.5 m/s flow velocity. The median collapse flow velocity is generally small at different years when the flow height reaches to the deck. Fig. 16(a) illustrates that the median collapse flow velocity is 10.2 m/s at year 0 and 9.9 m/s at year 100 for 7.0 m inundation depth flow. Fig. 17(a) shows that the median collapse flow velocity is 6.7 m/s at year 0 and 6.4 m/s at year 100 for 7.8 m inundation depth flow. The median collapse flow velocity does not change significantly over time; however, due to the low required flow velocity, the bridge is more vulnerable subjected to tsunami hazards with flow depths reaching to the deck.

Although the collapse failure probability of the bridge increases with the increasing of flow velocity, the flow velocity of the tsunami flow is constrained to a specific value for a given flow depth (Alam et al. 2018)

$$u_{\max} = F_r\sqrt{gh} \tag{24}$$

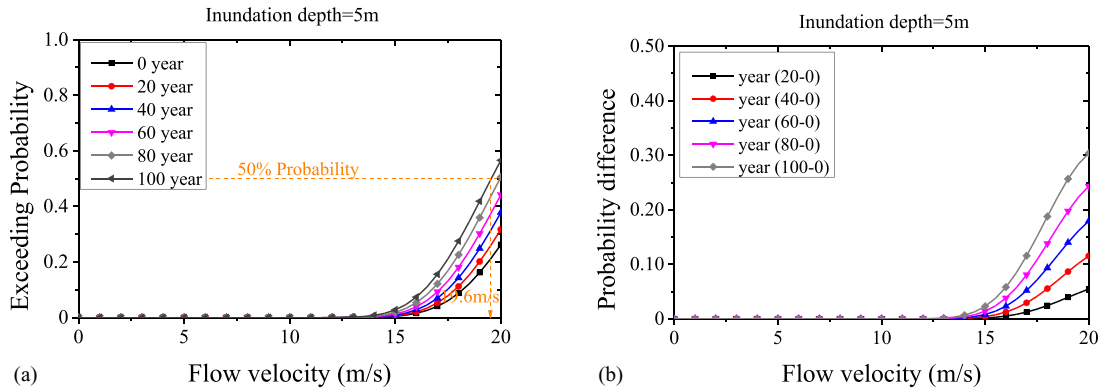

Fig. 14. Collapse failure probability and failure probability difference of the bridge for 5.0 m inundation depth: (a) collapse failure probability curves; and (b) failure probability difference.

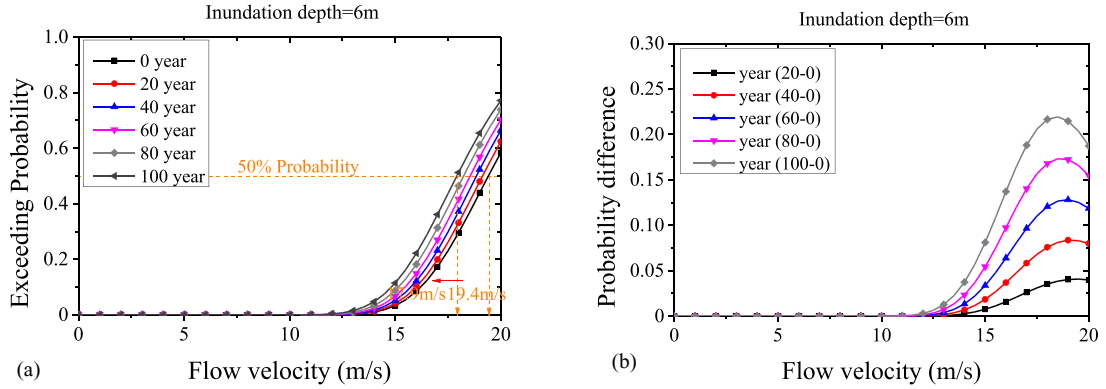

Fig. 15. Collapse failure probability and failure probability difference of the bridge for 6.0 m inundation depth: (a) collapse failure probability curves; and (b) failure probability difference.

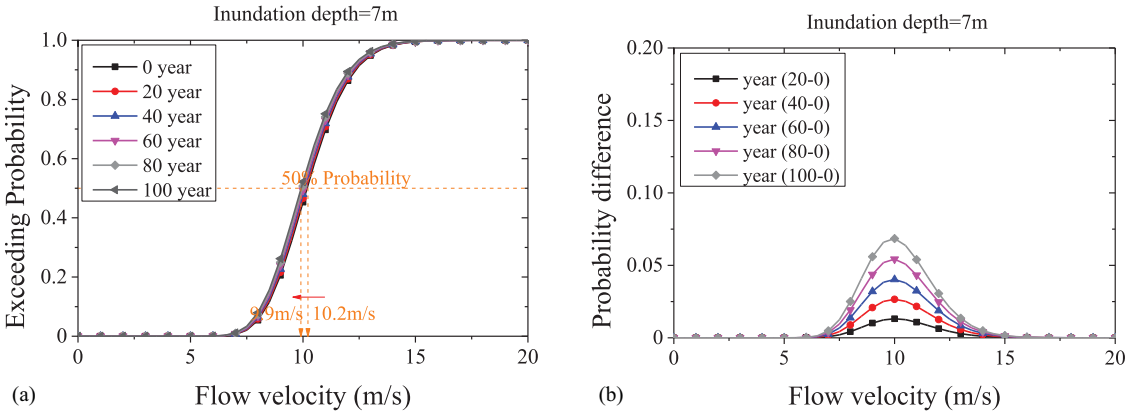

Fig. 16. Collapse failure probability and failure probability difference of the bridge for 7.0 m inundation depth: (a) collapse failure probability curves; and (b) failure probability difference.

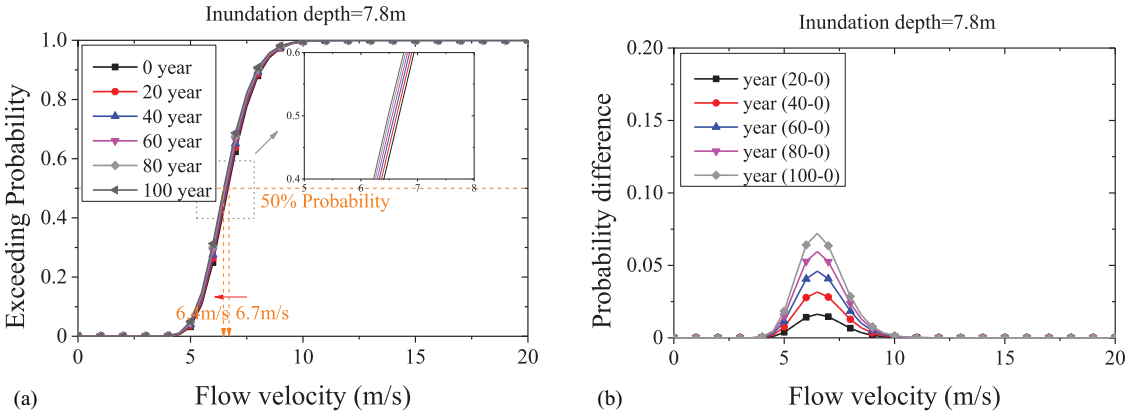

Fig. 17. Collapse failure probability and failure probability difference of the bridge for 7.8 m inundation depth: (a) collapse failure probability curves; and (b) failure probability difference.

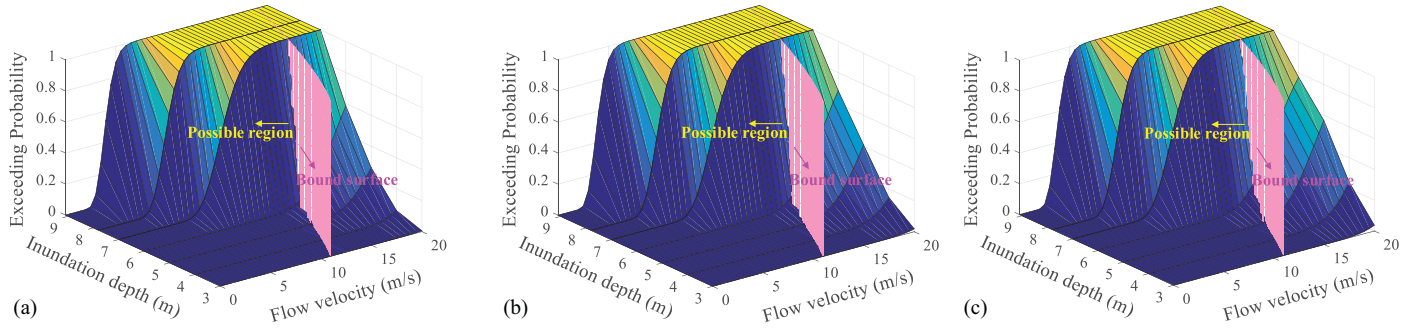

Fig. 18. Time-dependent collapse fragility surface with the bounded surface: (a) 0 year; (b) 50 year; and (c) 100 year.

Table 3. Failure probabilities of the bridge at various hazard conditions

Tsunami hazard levels	Failure probability		
	0 year (%)	50 year (%)	100 year (%)
Tsunami with $h = 5.0$ m, $u = 14.1$ m/s	0.13	0.29	0.78
Tsunami with $h = 6.0$ m, $u = 15.5$ m/s	5.50	9.18	16.36
Tsunami with $h = 7.0$ m, $u = 16.7$ m/s	100	100	100

where h = flow depth, g = gravity acceleration, u_{max} = possible maximum flow velocity, and F_r = Froude number. Fig. 18 shows the time-dependent collapse fragility surface with the bounded surface. F_r is taken as 2.0 following (Alam et al. 2018) for the bounded surface. It is shown in Fig. 18 that the possible region increases with the inundation depth.

From the possible region of the collapse fragility surface, the effect of tsunami hazard levels on the failure probability of the bridge can be assessed. Table 3 presents the failure probabilities of the bridge at various tsunami hazard conditions for three

different years. For the tsunami hazard considered, the flow velocity is taken as the maximum possible flow velocity calculated based on Eq. (24) with $F_r = 2.0$. It can be seen from Table 3 that the tsunami flow depth significantly affects the failure probability of the bridge. At time year 0, the failure probability of the bridge is 0.13% for 5.0 m depth flow, and failure probability will increase to 5.50% for 6.0 m depth flow and 100% for 7.0 m depth flow. With time increases, the failure probability slightly increases. For instance, for 6.0 m depth flow, the failure probability will increase from 5.50% at time year 0 to 16.36% at time year 100.

Concluding Remarks

In the present study, the time-dependent collapse fragility analysis is conducted to investigate the life-cycle performance of aging RC bridges subjected to tsunami hazards. The chloride-induced corrosion is considered to be the deterioration mechanism and, via corrosion modeling, the time-dependent corrosion levels of reinforcements are derived. The nonlinear TPO analysis is used to investigate the bridge damage under tsunami loading. The tsunami collapse fragility curves are calculated assuming a lognormal distribution and, with the quadratic model for the median and standard deviation of tsunami intensity, the time-dependent tsunami collapse fragility curves can be efficiently calculated. From the analysis results, some conclusions can be obtained as:

- Tsunami inundation depth can affect the bridge column failure modes. For low flow depth, the columns generally fail in shear modes, while with the increasing of flow depth, the failure mode of the column shifts to flexure. Corrosion can also affect the columns failure modes. Due to the severer corrosion levels of transverse reinforcements than longitudinal reinforcements, the failure mode of the column may shift form flexure to shear because of the severer shear capacity degradation.
- Due to the sudden jump of the breadth-facing tsunami flow, the tsunami loadings imposed on bridge significantly increase and a clear jump of failure probability for inundation depth from below to above the deck can be observed. For inundation depth below the deck, the median collapse flow velocity is larger than 19.0 m/s and unlikely to occur for tsunami events. However, for inundation depths reaching to the deck, the median collapse flow velocity can be reduced to smaller than 10.2 m/s, which could be within the range for recent tsunami events.
- The collapse failure probability and failure probability difference increase over time due to corrosion effects for lower inundation depths. While for higher inundation depths where columns fail in flexure, the effects of corrosion are minor because of the lower corrosion levels of longitudinal reinforcements.
- Tsunami hazard levels and aging time can both affect the failure probability of the bridge. At the maximum possible flow velocity for variant flow depths, the failure probability of the bridge is 0.13% for 5.0 m depth flow at time year 0 and increase to 5.50% for 6.0 m depth flow and 100% for 7.0 m depth flow. With time increases, the failure probability also increases. For 6.0 m depth flow, the failure probability of the bridge will increase from 5.50% at time year 0 to 16.36% at time year 100.

Further work on the research topic would consider other tsunami forces, such as debris impact forces and debris damming forces in order to develop more reliable fragility curves for RC bridges under tsunami hazards. The effects of corrosion on other bridge components with different bridge configurations are also of research interests.

Appendix. Corrosion Modeling Parameters for Assumed Marine Tidal Zone

Parameter	Value	Unit
w/c	0.5	—
D_0	473	mm^2/year
k_e	0.924	—
k_t	0.832	—
k_c	1.0	—
t_0	28	Day
n	0.362	—
A_{cs}	7.758	—
ε_{CS}	0	—
C_{cr}	0.9	Mass % of binder

Source: Data from Choe et al. (2009).
Note: C_S is computed as: $C_S = A_{cs}(w/b) + \varepsilon_{cs}$.

Data Availability Statement

All data, models, or codes that support the findings of this study are available from the corresponding author upon reasonable request.

Acknowledgments

The authors acknowledge financial support from the National Natural Science Foundation of China (Nos. 51838004 and 51525801). The opinions and conclusions presented in this paper are those of the authors and do not necessarily reflect the views of the sponsoring organizations.

References

Akiyama, M., D. M. Frangopol, M. Arai, and S. Koshimura. 2012. "Probabilistic assessment of structural performance of bridges under tsunami hazard." In *Structures Congress 2012*, edited by J. Carrato, and J. Burns, 1919–1928. Reston, VA: ASCE.

Akiyama, M., D. M. Frangopol, M. Arai, and S. Koshimura. 2013. "Reliability of bridges under tsunami hazards: Emphasis on the 2011 Tohoku-Oki earthquake." *Earthquake Spectra* 29 (S1): 295–314. https://doi.org/10.1193/1.4000112.

Akiyama, M., D. M. Frangopol, and H. Ishibashi. 2020. "Toward life-cycle reliability-, risk- and resilience-based design and assessment of bridges and bridge networks under independent and interacting hazards: Emphasis on earthquake, tsunami and corrosion." *Struct. Infrastruct. Eng.* 16 (1): 26–50. https://doi.org/10.1080/15732479.2019.1604770.

Akiyama, M., D. M. Frangopol, and H. Matsuzaki. 2011. "Life-cycle reliability of RC bridge piers under seismic and airborne chloride hazards." *Earthquake Eng. Struct. Dyn.* 40 (15): 1671–1687. https://doi.org/10.1002/eqe.1108.

Alam, M. S., A. R. Barbosa, M. H. Scott, D. T. Cox, and J. W. van de Lindt. 2018. "Development of physics-based tsunami fragility functions considering structural member failures." *J. Struct. Eng.* 144 (3): 04017221. https://doi.org/10.1061/(ASCE)ST.1943-541X.0001953.

Alipour, A., B. Shafei, and M. Shinozuka. 2011. "Performance evaluation of deteriorating highway bridges located in high seismic areas." *J. Bridge Eng.* 16 (5): 597–611. https://doi.org/10.1061/(ASCE)BE.1943-5592.0000197.

Arnason, H., C. Petroff, and H. Yeh. 2009. "Tsunami bore impingement onto a vertical column." *J. Disaster Res.* 4 (6): 391–403. https://doi.org/10.20965/jdr.2009.p0391.

Asadollahi, N., I. Nistor, and A. Mohammadian. 2019. "Numerical investigation of tsunami bore effects on structures, part I: Drag coefficients." *Nat. Hazards* 96 (1): 285–309. https://doi.org/10.1007/s11069-018-3542-2.

Attary, N., V. U. Unnikrishnan, J. W. van de Lindt, D. T. Cox, and A. R. Barbosa. 2017. "Performance-based tsunami engineering methodology for risk assessment of structures." *Eng. Struct.* 141: 676–686. https://doi.org/10.1016/j.engstruct.2017.03.071.

Azadbakht, M., and S. C. Yim. 2015. "Simulation and estimation of tsunami loads on bridge superstructures." *J. Waterw. Port Coastal Ocean Eng.* 141 (2): 04014031. https://doi.org/10.1061/(ASCE)WW.1943-5460.0000262.

Azadbakht, M., and S. C. Yim. 2016. "Estimation of Cascadia local tsunami loads on Pacific Northwest bridge superstructures." *J. Bridge Eng.* 21 (2): 04015048. https://doi.org/10.1061/(ASCE)BE.1943-5592.0000755.

Barbato, M., A. Zona, and J. P. Conte. 2014. "Probabilistic nonlinear response analysis of steel-concrete composite beams." *J. Struct. Eng.* 140 (1): 04013034. https://doi.org/10.1061/(ASCE)ST.1943-541X.0000803.

Biondini, F., E. Camnasio, and A. Palermo. 2014. "Lifetime seismic performance of concrete bridges exposed to corrosion." *Struct. Infrastruct. Eng.* 10 (7): 880–900. https://doi.org/10.1080/15732479.2012.761248.

Bricker, J. D., and A. Nakayama. 2014. "Contribution of trapped air, deck superelevation, and nearby structures to bridge deck failure during a tsunami." *J. Hydraul. Eng.* 140 (5): 05014002. https://doi.org/10.1061/(ASCE)HY.1943-7900.0000855.

Cheng, H., H.-N. Li, Y. B. Yang, and D.-S. Wang. 2019. "Seismic fragility analysis of deteriorating RC bridge columns with time-variant capacity index." *Bull. Earthquake Eng.* 17 (7): 4247–4267. https://doi.org/10.1007/s10518-019-00628-x.

Choe, D.-E., P. Gardoni, D. Rosowsky, and T. Haukaas. 2009. "Seismic fragility estimates for reinforced concrete bridges subject to corrosion." *Struct. Saf.* 31 (4): 275–283. https://doi.org/10.1016/j.strusafe.2008.10.001.

Choi, E., R. DesRoches, and B. Nielson. 2004. "Seismic fragility of typical bridges in moderate seismic zones." *Eng. Struct.* 26 (2): 187–199. https://doi.org/10.1016/j.engstruct.2003.09.006.

Cui, F., H. Zhang, M. Ghosn, and Y. Xu. 2018. "Seismic fragility analysis of deteriorating RC bridge substructures subject to marine chloride-induced corrosion." *Eng. Struct.* 155: 61–72. https://doi.org/10.1016/j.engstruct.2017.10.067.

Deng, P., C. Zhang, S. Pei, and Z. Jin. 2018. "Modeling the impact of corrosion on seismic performance of multi-span simply-supported bridges." *Constr. Build. Mater.* 185: 193–205. https://doi.org/10.1016/j.conbuildmat.2018.07.015.

Du, Y. G., L. A. Clark, and A. H. C. Chan. 2005a. "Residual capacity of corroded reinforcing bars." *Mag. Concr. Res.* 57 (3): 135–147. https://doi.org/10.1680/macr.2005.57.3.135.

Du, Y. G., L. A. Clark, and A. H. C. Chan. 2005b. "Effect of corrosion on ductility of reinforcing bars." *Mag. Concr. Res.* 57 (7): 407–419. https://doi.org/10.1680/macr.2005.57.7.407.

FEMA. 2012. *Guidelines for design of structures for vertical evacuation from tsunamis*. FEMA P-646. Washington, DC: FEMA.

FEMA. 2013. *Tsunami methodology technical manual*. Washington, DC: FEMA.

Feng, D. C., Z. Wang, and G. Wu. 2019. "Progressive collapse performance analysis of precast reinforced concrete structures." *Struct. Des. Tall Spec. Build.* 28 (5): e1588. https://doi.org/10.1002/tal.1588.

FHWA (Federal Highway Administration). 2019. "Bridge condition by highway system." Accessed June 20, 2019. https://www.fhwa.dot.gov/bridge/britab.cfm.

Fritz, H. M., D. A. Phillips, A. Okayasu, T. Shimozono, H. Liu, F. Mohammed, V. Skanavis, C. E. Synolakis, and T. Takahashi. 2012. "The 2011 Japan tsunami current velocity measurements from survivor videos at Kesennuma Bay using LiDAR." *Geophys. Res. Lett.* 39 (7): L00G23. https://doi.org/10.1029/2011GL050686.

Fujima, K., F. Achmad, Y. Shigihara, and N. Mizutani. 2009. "Estimation of tsunami force acting on rectangular structures." *J. Disaster Res.* 4 (6): 404–409. https://doi.org/10.20965/jdr.2009.p0404.

Ghosh, J., and J. E. Padgett. 2010. "Aging considerations in the development of time-dependent seismic fragility curves." *J. Struct. Eng.* 136 (12): 1497–1511. https://doi.org/10.1061/(ASCE)ST.1943-541X.0000260.

Ghosh, J., and P. Sood. 2016. "Consideration of time-evolving capacity distributions and improved degradation models for seismic fragility assessment of aging highway bridges." *Reliab. Eng. Syst. Saf.* 154: 197–218. https://doi.org/10.1016/j.ress.2016.06.001.

Gidaris, I., J. E. Padgett, A. R. Barbosa, S. Chen, D. Cox, B. Webb, and A. Cerato. 2017. "Multiple-hazard fragility and restoration models of highway bridges for regional risk and resilience assessment in the United States: State-of-the-art review." *J. Struct. Eng.* 143 (3): 04016188. https://doi.org/10.1061/(ASCE)ST.1943-541X.0001672.

Guo, A., W. Yuan, C. Lan, X. Guan, and H. Li. 2015. "Time-dependent seismic demand and fragility of deteriorating bridges for their residual service life." *Bull. Earthquake Eng.* 13 (8): 2389–2409. https://doi.org/10.1007/s10518-014-9722-x.

Hayashi, H. 2013. "Study on tsunami wave force acting on a bridge superstructure." In *Proc., 29th US-Japan Bridge Engineering Workshop*, 11–13. Tsukuba, Japan: Task Committee G (Transportation Systems).

Hsu, T. T. C., and Y.-L. Mo. 2010. *Unified theory of concrete structures*. Chichester, UK: Wiley.

Istrati, D., and I. Buckle. 2019. "Role of trapped air on the tsunami-induced transient loads and response of coastal bridges." *Geosciences* 9 (4): 191. https://doi.org/10.3390/geosciences9040191.

Istrati, D., I. Buckle, S. Yim, and P. Lomonaco. 2018. "Deciphering the tsunami wave impact and associated connection forces in opengirder coastal bridges." *J. Mar. Sci. Eng.* 6 (4): 148. https://doi.org/10.3390/jmse6040148.

Jeon, J.-S., R. DesRoches, and D. H. Lee. 2016. "Post-repair effect of column jackets on aftershock fragilities of damaged RC bridges subjected to successive earthquakes." *Earthquake Eng. Struct. Dyn.* 45 (7): 1149–1168. https://doi.org/10.1002/eqe.2700.

Jeon, J.-S., S. Mangalathu, and S.-Y. Lee. 2019. "Seismic fragility curves for California concrete bridges with flared two-column bents." *Bull. Earthquake Eng.* 17 (7): 4299–4319. https://doi.org/10.1007/s10518-019-00621-4.

Kajitani, Y., S. E. Chang, and H. Tatano. 2013. "Economic impacts of the 2011 Tohoku-Oki earthquake and tsunami." *Earthquake Spectra* 29 (S1): 457–478. https://doi.org/10.1193/1.4000108.

Koshimura, S., Y. Namegaya, and H. Yanagisawa. 2009. "Tsunami fragility-a new measure to identify tsunami damage." *J. Disaster Res.* 4 (6): 479–488. https://doi.org/10.20965/jdr.2009.p0479.

Lau, T. L., T. Ohmachi, S. Inoue, and P. Lukkunaprasit. 2011. "Experimental and numerical modeling of tsunami force on bridge decks." In *Tsunami-A growing disaster*, edited by M. Mokhtari, 105–130. Vienna, Austria: INTECH Open Access Publisher.

Leelawat, N., A. Suppasri, O. Murao, and F. Imamura. 2016. "A study on the influential factors on building damage in Sri Lanka during the 2004 Indian Ocean Tsunami." *J. Earthquake Tsunami* 10 (2): 1640001. https://doi.org/10.1142/S1793431116400017.

Mander, J. B., M. J. N. Priestley, and R. Park. 1988. "Theoretical stress-strain model for confined concrete." *J. Struct. Eng.* 114 (8): 1804–1826. https://doi.org/10.1061/(ASCE)0733-9445(1988)114:8(1804).

Mangalathu, S. 2017. "Performance based grouping and fragility analysis of box girder bridges in California." Ph.D. thesis, School of Civil and Environmental Engineering, Georgia Institute of Technology.

Mangalathu, S., E. Choi, H. C. Park, and J.-S. Jeon. 2018. "Probabilistic seismic vulnerability assessment of tall horizontally curved concrete bridges in California." *J. Perform. Constr. Facil* 32 (6): 04018080. https://doi.org/10.1061/(ASCE)CF.1943-5509.0001231.

Mangalathu, S., and J. S. Jeon. 2019. "Stripe-based fragility analysis of multispan concrete bridge classes using machine learning techniques." *Earthquake Eng. Struct. Dyn.* 48 (11): 1238–1255. https://doi.org/10.1002/eqe.3183.

Mazzoni, S., F. McKenna, M. H. Scott, and G. L. Fenves. 2005. *Opensees command language manual*. Berkeley, CA: Pacific Earthquake Engineering Research (PEER) Center.

Medina, S., J. Lizarazo-Marriaga, M. Estrada, S. Koshimura, E. Mas, and B. Adriano. 2019. "Tsunami analytical fragility curves for the Colombian Pacific coast: A reinforced concrete building example." *Eng. Struct.* 196: 109309. https://doi.org/10.1016/j.engstruct.2019.109309.

Ramanathan, K. N. 2012. "Next generation seismic fragility curves for California bridges incorporating the evolution in seismic design philosophy." Ph.D. thesis, School of Civil and Environmental Engineering, Georgia Institute of Technology.

Ranjkesh, S. H., P. Asadi, and A. Z. Hamadani. 2019. "Seismic collapse assessment of deteriorating RC bridges under multiple hazards during their life-cycle." *Bull. Earthquake Eng.* 17 (9): 5045–5072. https://doi.org/10.1007/s10518-019-00647-8.

Scott, M. H., and H. B. Mason. 2017. "Constant-ductility response spectra for sequential earthquake and tsunami loading." *Earthquake Eng. Struct. Dyn.* 46 (9): 1549–1554. https://doi.org/10.1002/eqe.2871.

Shafiei, S., B. W. Melville, and A. Y. Shamseldin. 2016. "Experimental investigation of tsunami bore impact force and pressure on a square prism." *Coastal Eng.* 110: 1–16. https://doi.org/10.1016/j.coastaleng.2015.12.006.

Shamsabadi, A., P. Khalili-Tehrani, J. P. Stewart, and E. Taciroglu. 2010. "Validated simulation models for lateral response of bridge abutments with typical backfills." *J. Bridge Eng.* 15 (3): 302–311. https://doi.org/10.1061/(ASCE)BE.1943-5592.0000058.

Shoji, G., and T. Moriyama. 2007. "Evaluation of the structural fragility of a bridge structure subjected to a tsunami wave load." *J. Nat. Disaster Sci.* 29 (2): 73–81. https://doi.org/10.2328/jnds.29.73.

Vishwanath, B. S., and S. Benerjee. 2019. "Life-cycle resilience of aging bridges under earthquakes." *J. Bridge Eng.* 24 (11): 04019106. https://doi.org/10.1061/(ASCE)BE.1943-5592.0001491.

Vu, K. A. T., and M. G. Stewart. 2000. "Structural reliability of concrete bridges including improved chloride-induced corrosion models." *Struct. Saf.* 22 (4): 313–333. https://doi.org/10.1016/S0167-4730(00)00018-7.

Vu, N. S., and B. Li. 2018a. "Seismic performance of flexural reinforced concrete columns with corroded reinforcement." *ACI Struct. J.* 115 (5): 1253–1266. https://doi.org/10.14359/51702372.

Vu, N. S., and B. Li. 2018b. "Seismic performance assessment of corroded reinforced concrete short columns." *J. Struct. Eng.* 144 (4): 04018018. https://doi.org/10.1061/(ASCE)ST.1943-541X.0001994.

Wei, Z., R. A. Dalrymple, A. Hérault, G. Bilotta, E. Rustico, and H. Yeh. 2015. "SPH modeling of dynamic impact of tsunami bore on bridge piers." *Coastal Eng.* 104: 26–42. https://doi.org/10.1016/j.coastaleng.2015.06.008.

Winter, A. O., M. R. Motley, and M. O. Eberhard. 2018. "Tsunami-like wave loading of individual bridge components." *J. Bridge Eng.* 23 (2): 04017137. https://doi.org/10.1061/(ASCE)BE.1943-5592.0001177.

Xu, G., and C. S. Cai. 2015. "Numerical simulations of lateral restraining stiffness effect on bridge deck–wave interaction under solitary waves." *Eng. Struct.* 101: 337–351. https://doi.org/10.1016/j.engstruct.2015.07.031.

Yanweerasak, T., W. Pansuk, M. Akiyama, and D. M. Frangopol. 2018. "Life-cycle reliability assessment of reinforced concrete bridges under multiple hazards." *Struct. Infrastruct. Eng.* 14 (7): 1011–1024. https://doi.org/10.1080/15732479.2018.1437640.

Yeh, H., S. Sato, and Y. Tajima. 2013. "The 11 March 2011 East Japan earthquake and tsunami: Tsunami effects on coastal infrastructure and buildings." *Pure Appl. Geophys.* 170 (6): 1019–1031. https://doi.org/10.1007/s00024-012-0489-1.

Yim, S. C., Y. Wei, M. Azadbakht, S. Nimmala, and T. Potisuk. 2015. "Case study for tsunami design of coastal infrastructure: Spencer Creek bridge, Oregon." *J. Bridge Eng.* 20 (1): 05014008. https://doi.org/10.1061/(ASCE)BE.1943-5592.0000631.